Since January 2020 Elsevier has created a COVID-19 resource centre with free information in English and Mandarin on the novel coronavirus COVID-19. The COVID-19 resource centre is hosted on Elsevier Connect, the company's public news and information website.

Biochimica et Biophysica Acta 1808 (2011) 572–579

Contents lists available at ScienceDirect

Biochimica et Biophysica Acta

journal homepage: www.elsevier.com/locate/bbamem

ORF8a of SARS-CoV forms an ion channel: Experiments and molecular dynamics simulations

Cheng-Chang Chen [a], Jens Krüger [a], Issara Sramala [b], Hao-Jen Hsu [a], Peter Henklein [c], Yi-Ming Arthur Chen [d], Wolfgang B. Fischer [a,*]

[a] Institute of Biophotonics, School of Biomedical Science and Engineering, National Yang-Ming University, 155, Li-Nong St., Sec. 2, Taipei, 112, Taiwan
[b] National Nanotechnology Center, NSTDA, Thailand
[c] Institute of Biochemistry, Humboldt University, Berlin, Germany
[d] AIDS Prevention and Research Center, NYMU, Taiwan

ARTICLE INFO

Article history:
Received 11 June 2010
Received in revised form 27 July 2010
Accepted 2 August 2010
Available online 12 August 2010

Keywords:
SARS-CoV
ORF8a
Ion channel
Molecular dynamics
Bilayer recording

ABSTRACT

ORF8a protein is 39 residues long and contains a single transmembrane domain. The protein is synthesized using solid phase peptide synthesis and reconstituted into artificial lipid bilayers that forms cation-selective ion channels with a main conductance level of 8.9 ± 0.8 pS at elevated temperature (38.5 °C). Computational modeling studies including multi nanosecond molecular dynamics simulations in a hydrated POPC lipid bilayer are done with a 22 amino acid transmembrane helix to predict a putative homooligomeric helical bundle model. A structural model of a pentameric bundle is proposed with cysteines, serines and threonines facing the pore.

1. Introduction

Coronavirus (Co-V) is the causal agent responsible for the severe acute respiratory syndrome (SARS) [1,2]. The 29.7 kb genome structure of SARS-CoV contains a single positive stranded RNA harboring 14 open reading frames (ORFs) which are translated into a large polyprotein which is processed by viral encoded protease to derive the individual proteins [3,4]. One of the structural proteins from ORF8a encodes a membrane-associated protein with 39 amino acids and contains a single transmembrane domain (TMD) with a length of approximately 22 residues [5]. ORF 8a has been proposed not only to enhance viral replication but also to induce apoptosis through a mitochondria-dependent pathway [5]. Its topology and biological function remains yet unknown.

Viral channel forming proteins (VCPs) participate in several viral functions. They change chemical or electrochemical gradients by altering ion permeability of the lipid membrane and modulate cellular response by interacting with membrane proteins of the host [6–9]. Several VCPs have been detected as ion channels, especially when reconstituted into lipid bilayers. VCPs are suggested to be encoded in the genomes of enveloped and naked viruses and also chlorella plant virus PBCV-1. VCPs, like host channels and pore forming microbial peptides [10–13], have to assemble to form homo oligomeric bundles. They are found to consist of approximately 80 to 100 amino acids. Exceptions emerge with the discovery of 3a from SARS-CoV with a length of 274 amino acids [14] and, based on this study, of ORF8a with 39 amino acids.

In the presented study, we demonstrate experimentally that ORF8a forms channels when reconstituted into artificial lipid bilayers at elevated temperature (38.5 °C). It is suggested that ORF8a$_{3-20}$ is part of the TMD and multi nanosecond molecular dynamic simulations of ORF8a$_{3-20}$ within a POPC bilayer are undertaken. A set of different oligomeric bundle models raging from 4 to 6 units is generated. The generation of computational bundle models follows the 'two stage model' [15,16]. In short, this model suggests that the secondary structure of a protein is generated prior to its tertiary or quaternary structure. The identification and structural characterization of the new ion channel protein — ORF8a from SARS-CoV — will be helpful for the design of novel drugs against SARS.

2. Methods

2.1. Peptide synthesis

ORF8a, MKLLIVLTCI^{10} SLCSCICTVV^{20} QRCASNKPHV^{30} LEDPCKVQ^{39} was synthesized using solid phase peptide synthesis on a 433A synthesizer using Fmoc-Chemistry and HBtU as coupling reagent. The following side-chain-protecting groups were used: t-Butyl for Ser and

* Corresponding author. Tel.: +886 2 2826 7394; fax: +886 2 28235460.
E-mail address: wfischer@ym.edu.tw (W.B. Fischer).

0005-2736/$ – see front matter © 2010 Elsevier B.V. All rights reserved.
doi:10.1016/j.bbamem.2010.08.004

Thr, trityl for Cys, His, Asn and Gln, Boc for Lys and Pbf for Arg. After completion of the synthesis, the peptide was cleaved from the resin using 95% TFA/water and 3% triisopropylsilane for 3 h at room temperature. After cleavage the crude peptide was precipitated with ether and lyophilized. The crude peptide was purified by preparative RP-HPLC on a 21 × 300 mm Kromasil column with a flow rate of 70 ml/min. Peaks were detected by UV at 220 nm and the separated product was identified by mass spectrometry.

2.2. Reconstitution and channel recordings

Channel recordings of ORF8a were made with the protein reconstituted into lipid bilayer mixture of POPE (1-palmitoyl-2-oleoyl-*sn*-glycero-3-phosphoethanolamine) and DOPC (1,2-dioleoyl-*sn*-glycero-3-phosphocholine) (1:4 (volume), total lipid 5 mg/ml). Lipids were dissolved in chloroform, dried under N_2 gas and re-suspended in pentane and decane 9:1. Approximately 1 μl lipid suspension was brushed over the Delrin cup aperture (diameter 150 μl) and dried. Then 3 μl of peptide dissolved in trifluoroethanol (TFE) were added onto the aperture in the same way as the lipids. The lipid bilayer was formed by raising the level of the buffer (300 mM or 30 mM KCl, 5 mM K-HEPES, pH = 7.05) of both *trans*-(ground) and *cis*-side (head stage). The current response was recorded using Planar Lipid Bilayer Workstation from Warner Instruments with a BC-353 amplifier and 1440A data acquisition system. Temperature was set to 38.5 °C using a Bipolar Temperature Controller Model CL-100 from Warner Instruments. A constant positive voltage of 70 mV (*cis*-side) was applied during lipid bilayer formation to achieve an asymmetric orientation of the peptides within the bilayer [17]. Records were filtered with 10 Hz using a Bessel-8-pole low pass filter, digitized at 10 Hz and stored for further analysis.

Experiments have been repeated in the presence of the reducing agent dithiothreitol (DTT) with the peptide dissolved in TFE containing 50 mM DTT.

2.3. Computational methods

The application of several transmembrane (TM) prediction tools: DAS [18], TMHMM [19], TMpred [20], SPLIT4.0 [21] and SOSUI [22], which assume helical TM segments, have been used to detect the TM helical segments of the protein. An ideal helix of TMD of ORF8a (LLIVLTCI[10] SLCSCICTVV[20], $8a_{3-20}$) has been created using integrated protein builder of MOE (www.chemcomp.com). The helix was embedded into a lipid bilayer (POPC). Overlapping lipid molecules were removed using the MOE suite. The lipid–peptide system was then further processed using GROMACS-3.3 (www.gromacs.org). The topology and structure of the POPC bilayer was prepared as described elsewhere [23]. The lipid–peptide system was hydrated and a short minimization routine using steepest descent and conjugate gradients followed to remove unfavorable interactions. A short equilibration (500 ps) followed with the peptide restrained at the Cα atoms. At this stage the lipids were expected to surround the peptide adequately. In the production run (15 ns) all components were fully unrestrained.

The program g_covar from the GROMACS-3.3 package was used to perform Principal Component Analysis (PCA). The covariance matrix of positional variation was computed for the full 10 ns simulation length for the main-chain, based on the square fit of the Cα-atoms of TM residues 3–20. The rotational and translational motions were removed by fitting the peptide structure of each time frame to the initial structure.

The derived averaged monomer structure was then used in MOE to generate tetrameric (TBMs), pentameric (PBMs) and hexameric bundle models (HBMs) [24] by creating symmetric copies of monomeric units around a central pore axis. Degrees of freedom such as the rotational angle, inter-helical distance and tilt angle (further on referred to as 'tilt') were changed systematically. To sample the whole conformational space of the bundles each of the degrees of freedom is varied stepwise (inter-helical distance 0.1 Å, rotational angle 2° and tilt 2°). For each position the side chains were linked with the backbone. Side chain conformation is chosen to be the most likely one for the given backbone position and referenced in the MOE library. A short energy minimization (15 steps of steepest decent) followed the linking. Consequently the potential energy was calculated using the Engh-Huber force field implemented in MOE. More than one hundred thousand conformations are generated and stored in a database for further analysis.

Before embedding low energy models into lipid bilayers two amino acids residues of the protein were added at the N and C termini of each of the helices in each bundle model to account for the consequences of their interaction with the lipid bilayer during the simulation. Short ideal helices from Met-1 to Ile-5 and Thr-18 to Arg-22 were generated. They were aligned and superimposed with those residues from the bundle models. Those residues of the short helices which overlapped with the residues of the bundle models have been deleted and the remaining residues of the short helices conjoined with residues of the bundle models. This finally delivered bundle models of $8a_{1-22}$. The selected bundle models were then embedded into a pre-equilibrated (70 ns) hydrated POPC bilayer [23].

GROMACS-3.3 with the Gromos96 (ffG45a3) force field was used for the simulations with an integration step size of 2 fs. The temperature of the peptide, lipid and the water molecules were individually coupled to a Berendsen thermostat with a coupling time of 0.1 ps. Isotropic pressure coupling was used with a coupling time of 1.0 ps and a compressibility of 4.5e-5 bar^{-1}. Long range electrostatics was calculated using the particle-mesh Ewald (PME) algorithm with grid dimensions of 0.12 nm and interpolation order 4. Lennard–Jones and short-range Coulomb interactions were cut off at 1.4 and 0.8 nm, respectively. The simulation boxes contained around 26,011 atoms for

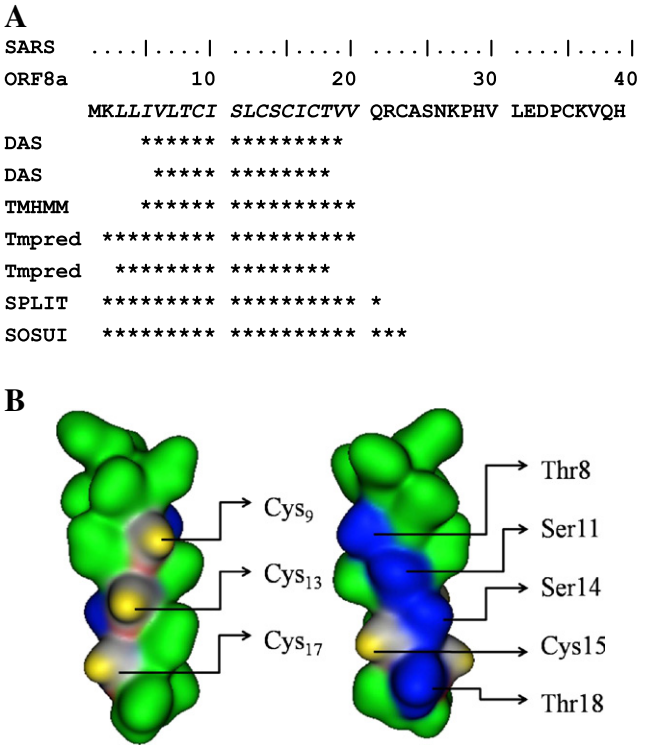

Fig. 1. Identification of the putative membrane-spanning domain of the 39 amino acid sequence of ORF8a using secondary structure prediction tools (A). Amino acids chosen to model a helical TMD are shown in italics. $ORF8a_{2-20}$ ideal helix including the bold residues shown in its 'Gaussian Contact' representation (MOE) (B). Hydrophilic and hydrophobic residues are highlighted in black and light gray, respectively.

the tetrameric models (protein 828 atoms, lipids 5824 atoms, water molecules 19,359 atoms), 26,218 atoms for the pentameric model (protein 1035 atoms) and 26,425 atoms for the hexameric models (protein 1242 atoms). Calculations of the root mean square deviations (RMSD) were based on the Cα atoms.

The simulations were run on a DELL Precision 490n workstation and a 28 core Opteron based compute cluster with Infiniband interconnects. All pictures were generated using xmgrace, VMD-1.8.6 and MOE-2007.09.

3. Results

Application of several TM prediction tools suggests a range of amino acids within the N terminal part of the protein (Fig. 1A). The longest stretch is suggested by SOSUI from Lys-2 to Ala-28 and the shortest stretch by DAS (Val-5 to Thr-18). All other programs place the start of the helix between residues Lys-2 to Ile-4 and the end between Thr-18 to Ala-28. For the experimental and computational investigations a consensus length of 18 residues from Leu-3 to Val-20 is chosen.

3.1. Channel recordings

Channel recordings of SARS ORF8a at a KCl concentration of 300 mM at 38.5 °C show frequent openings (Fig. 2A). The temperature has been chosen to simulate elevated body temperature occurring during fever. The lipid composition and their individual components have been proven successful in previous investigations [25]. DOPC is also successfully used in bilayer recordings [26] and is known to reduce packing density and enhance the integration of the peptide

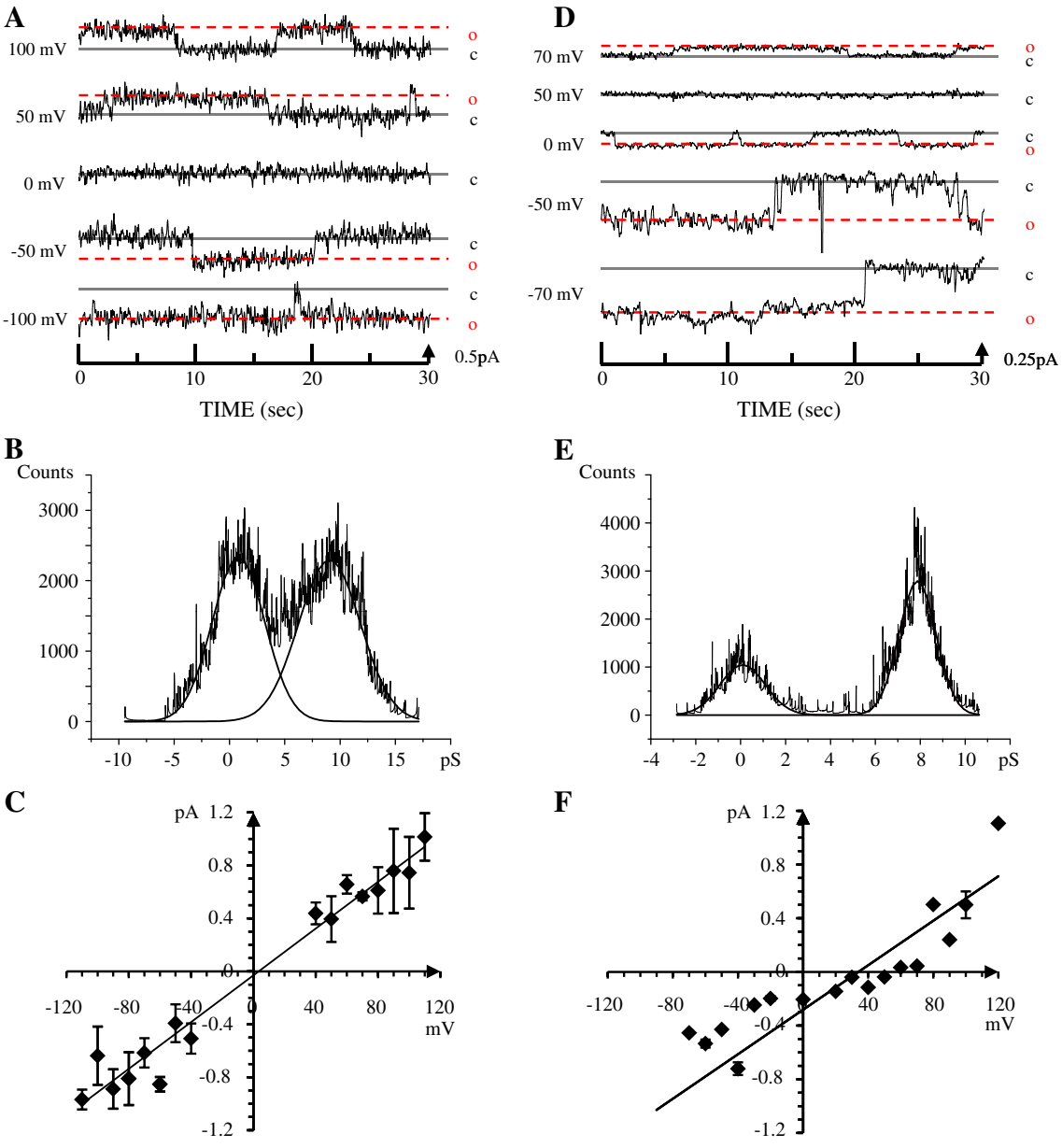

Fig. 2. Channel recordings of ORF8a peptide reconstituted into lipid bilayers and symmetric ion solution. Sample traces are shown at 0 mV, ±50 mV, and ±100 mV (A). The closed C (black line) and open states O (red dotted line) are indicated. Conductance histogram of a representative trace at a holding potential of +50 mV (B). Gaussian function indicates the conductance level. Current–voltage relation for all recordings with the estimated conductance (C). Sample traces (D), histogram (sample trace at +50 mV) (E) and current–voltage relation (F) of ORF8a peptide in an asymmetric ion solution (ten-fold).

into the bilayers [27]. The calculated conductance histograms of the recorded data enlighten a major conductance state of 8.8 ± 0.8 pS (Fig. 2B) and an ohmic behavior (Fig. 2C). Experiments have also been conducted in the presence of DTT (Fig. S1A), since the sequence of the peptide contains four cysteines (Fig. 1A). The overall behavior of the collected data remains the same as for the experiments without DTT, with a mean conductance of 8.9 ± 0.1 pS (Fig. S1B) and an ohmic channel behavior (Fig. S1C). All data in common is an increased open duration of the channels at negative potential.

Ion selectivity of ORF8a was evaluated with asymmetric buffer concentration (ten-fold in *trans* chamber) which shifts the potassium reversal potential independent of the presence of DTT to approximately 30–40 mV (Figs. 2D and S1D). The shift is indicative for a weak cation-selective channel. The data show a mean conductance of 8.3 ± 0.1 pS (Fig. 2E) and 8.6 ± 0.1 pS in the presence of DTT (Fig. S1E) and ohmic behavior (Figs. 2F and S1F).

3.2. Computational modeling

The idealized monomeric TM helix based on the consensus sequence Leu-3 to Val-20 (Fig. 1A) shows clustering of hydrophilic residues (Thr-8, Ser-11, Ser-14 and Thr-18) on one side suggesting that the four hydrophilic amino acids form the lumen of the pore in a homooligomeric helical bundle channel model. Four cysteines are forming a diagonal arrangement excluding any possibility for inter-helical Cys-bridges (Fig. 1B).

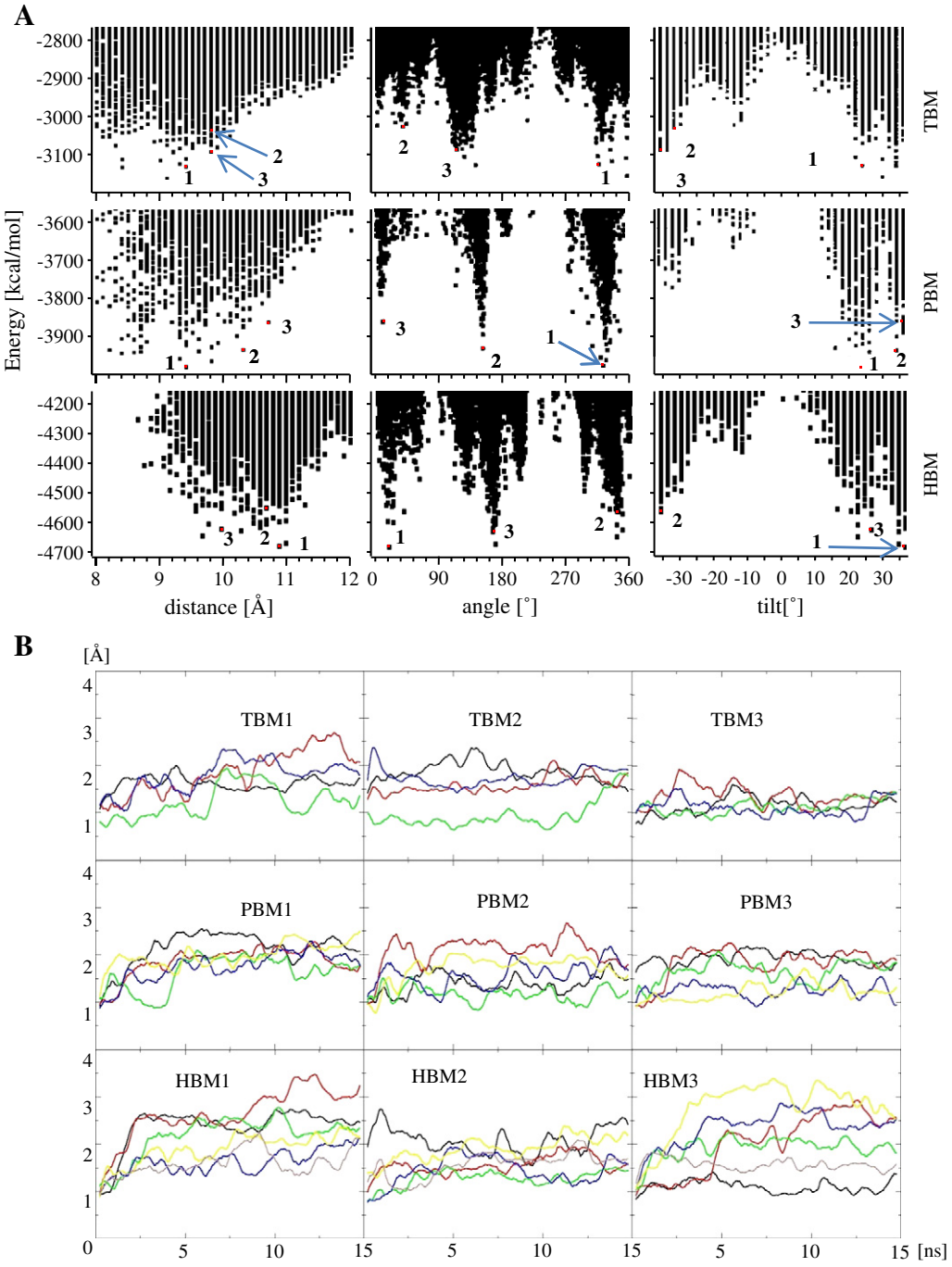

Fig. 3. Accumulated energy plots versus distance, angle or tilt of TBMs, PBMs and HBM2 (A). Three putative models taken for consequent MD simulations are indicated by numbers. Time dependent root mean square deviation (RMSD) of Cα backbones from the helical TBMs, PBMs and HBMs (B). The values for each of the monomers of the bundle models are shown in various colors. The plots have been smoothed by a 500 ps grid box average and a step width of 2 fs which leads to the omission of the first data points.

The generation of a series of assembled pore models follows a protocol which was reported earlier [23,24]. A single ideal helix ($8a_{3-20}$) is embedded in a hydrated lipid bilayer and undergoes a 10 ns MD simulation. An averaged helix from this simulation is generated based on a PCA analysis. Calculating the eigenvector quantifies the magnitude of the functional motion of the protein. Averaging over all structures of the first few eigenvectors delivers a structure of the helix which is the most likely one. This structure is then used to build the bundle models.

The use of the truncated part of 8a, $8a_{3-20}$, is rationalized by the understanding that the hydrophobic part of the TMD guides the assembly. In the current assembly protocol any unfavorable interactions due to hydrophilic residues at either end of the helix would be over emphasized. With $8a_{3-20}$ residues like Lys-2 and Arg-22 are not included during assembly.

Protein–protein interactions in respect to their potential and their individual three degrees of freedom are calculated. With decreasing inter-helical distance the energy values reach a minimum around 9.5 Å for the TBMs and PBMs (Fig. 3A). For both models some low energy models can also be observed around 8.5 Å. The HBMs have favorable energy values for inter-helical distances between 10 Å and 11 Å (Fig. 3A, left column). The lowest energy conformation in a minimum is seen as representative for similar conformations clustering around it.

Energy versus rotational angle correlation plots show three minima for all models which are separated by 150–160° (Fig. 3A, middle column). Each of the models adopts a minimum energy conformation for a left-handed tilt of around +25° to +35° (Fig. 3A, right column). For the right handed models a minimum is present at −10° and around −35°.

All bundles in common are rings of cysteines (Cys-13, -15, and -17), threonines (Thr-8), serines (Ser-11) and arginines (Arg-22, for PBM2 and PBM3 only) facing the lumen of the pore (Fig. 4). All hydrophilic and polarizable residues are separated by stretches of hydrophobic residues of various lengths. HBM1 and HBM3 exhibit the longest hydrophobic stretches within the lumen.

Three low energy pore models for each of the oligomers have been chosen for another 15 ns MD simulation to further minimize the proposed bundle models. The RMSD plots for all models rise during the first nanosecond to level off at around 1 to 3 Å (Fig. 3B). In one of the TBMs (TBM3) the spread of the RMSD values for the individual helices of the bundle is minimal, indicative for the helices retaining its starting structure (Fig. 3B, upper trace). For PBMs a moderate spread is observed (Fig. 3B, middle trace) whilst for the HBMs the largest spread can be detected (Fig. 3B, lower trace). Consequently, minor conformational adjustments away from the assembled structure occur.

The tilt angles averaged over the last 5 ns of each simulation are in the order of +30° to +40° and −25° to −30° (Table 1). The values are almost unchanged in respect to the values found during the assembly process (Fig. 3A). The tilts show the lowest deviations for TBMs and PBMs. The averaged inter-helical distance of the TBMs is between 6–7 Å (Table 1). For the PBMs the inter-helical distance is larger with values of 8 to 11 Å. In the HBMs the distance is around 9 Å, but shows large standard deviation. Visual inspection of all bundles reveals that most of the bundles fail to retain a circular pore assembly except TBM3, PBM2 and PBM3. The averaged minimum pore radii for the models are calculated (HOLE) to be (4.4 ± 0.2) Å for PBM2 and (3.5 ± 0.4) Å for PBM3 (Table 1). The minimum pore radius can be located with an accuracy of ±2.3 Å for PBM2 and ±2.7 Å for PBM3. For TBM3 the pore radius is calculated to be below 1.5 Å over the entire length of the pore which is too small to harbor any water molecules. As a result, water filled bundles of the TMD of ORF8a should adopt approximately a +40° tilt with a distance

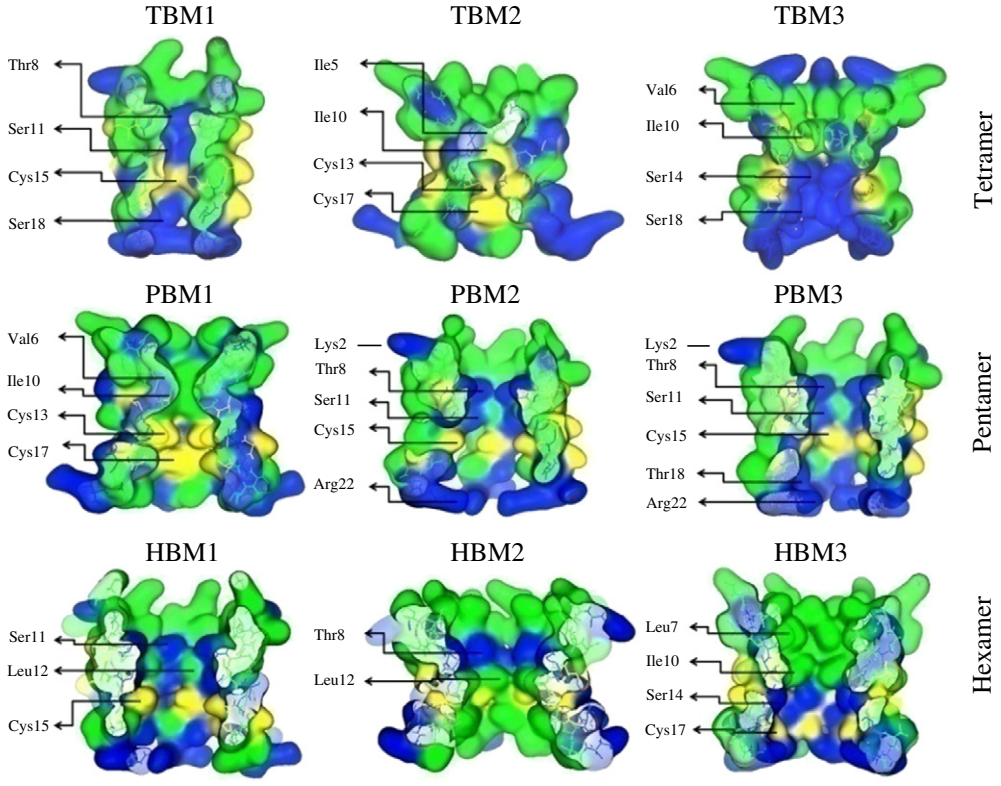

Fig. 4. Cross-section views of the putative TBMs, PBMs and HBMs as indicated by the numbers in Fig. 3A drawn in a 'Gaussian Contact' illustration (MOE). Hydrophilic residues (Thr-8, Ser-11, Ser-14 and Thr-18) are highlighted in blue and hydrophobic residues are shown in green. Cysteines are shown in yellow.

Table 1
Interhelical distances and tilt angles calculated between the centers of mass of each helix based on the Cα backbone atoms. Values are averaged over the last 5 ns of the 15 ns MD simulation runs. Minimum pore radius (MPR) is calculated as an average over six bundle models taken at 10, 11, 12, 13, 14 and 15 ns using the program HOLE [44].

Bundle models	Tilt [°]	Distance [Å]	MPR [nm]
TBM1	+30.1±6.1	7.1±1.4	–
TBM2	−28.8±9.8	6.2±1.9	–
TBM3	−24.6±7.3	6.3±1.1	–
PBM1	+30.3±10.6	8.7±3.6	–
PBM2	+42.8±4.9	11.1±0.7	4.4±0.2
PBM3	+37.6±5.4	10.4±1.1	3.5±0.4
HBM1	+26.5±11.0	9.0±4.6	–
HBM2	−25.8±11.9	9.4±3.5	–
HBM3	+30.9±12.1	9.2±3.4	–

between the helices in respect to their long axis of 11 Å (Fig. 5 for PBM2). With this large tilt hydrophilic residues Thr-8 and Ser-11 as well as Cys-15 of one helix form the hydrophilic stretch, whilst Ser-14 and Thr-18 are positioned at an inter-helical site. Lys-2 remains in an outward position 'snorkling' for the aqueous phase and the lipid head groups. The side chains of all the arginines (Arg-22) move from an all inward facing position to such a position that they point either outside the pore or towards the helix interface interacting with Gln-21 of the neighboring helix. All assemblies in common is also a line of cysteines (Cys-9, -13, and -17) in each helix at the outside of the bundle (Fig. 5, lower left). The hour glass shape of the water column is shown in Fig. 5 (lower right). The model underpins the necessity of a balanced pattern with alternating hydrophilic and hydrophobic residues mantling the pore to allow the existence of a continuous water column through the pore.

4. Discussion

4.1. Experimental data

The calculated conductance data of the OFR8a protein and its weak selectivity for cations is in accordance with findings of other viral channel forming proteins [25,28–30]. Selectivity has so far been reported for viral proteins with a single (e.g. Vpu from HIV-1) or double TM topology (e.g. p7 from HCV). Even though assuming that selectivity is coupled with flexibility and gating [31] it may be argued that with the helical topologies of a single and eventually double TMD no highly selective channels can be formed via self-assembly.

4.2. Evaluation of the computational protocol

In the protocol for the assembly of the TM helices of 8a a combination of molecular dynamics simulations with a fine grained positioning routine is used [23,24]. The positioning routine moves the helix on the bases of the backbone atoms to a specific position and consequently generates the side chains for each particular position. In this protocol a vacuum force field (Engh-Huber [32]) has been used. In another study, helix assembly undertaken in vacuum have been compared with data derived from MD simulations in a hydrated lipid bilayer and reported to explore the same conformational space [33]. This makes the use of vacuum conditions in combination with a fine grained search of the conformational space, a powerful tool [34]. Applying MD simulations after the assembly step aims to address for the specific environment of the bundle structure such as phospholipid head group region, hydrophobic slab as well as the hydrophilic environment within the lumen of the pore.

This protocol is along side of other protocols used to model TM helix assembly and bundle formation [35–39]. In some of these protocols a limited number of model structures is generated [35,36] and in other methods larger numbers of models are generated through extended simulation protocols and assessed [37,38]. All protocols so far do not account for kinetics of the assembly of larger units such as bundles or pores.

4.3. Inside the pore

The pore-lining pattern discovered in the model supports models from other viral channel forming proteins which have been derived using more biased model generation protocols in the past [40,41]. Based on experimental findings hydrophilic residues such as threonine, serine and charged residues such as aspartic and glutamic acids [42] as well as arginines and lysines, are seen as essential pore-lining motif for ion channels [43,44] and viral channel forming proteins [6,25,45]. A cysteine residue has been suggested to be at least transiently part of the pore-lining motif of the human concentrative nucleoside transporter 3 [46]. For the transient receptor potential (TRP) channels conserved cysteine residues within the pore region have been reported to be essential for channel function [47]. Also the AMPA receptor has a cysteine facing the lumen of the pore of the channel [48].

4.4. Outside the pore

The cysteines at the outside of the bundles may be able to lead to covalent linkages with host cell proteins or possibly an attachment to lipid rafts or other membrane based host cell factors. Also some of the threonines and serines are not solely pore lining but enable stabilize inter-helical interaction, a feature which has been suggested by modeling other bundle systems [49].

4.5. The shape of the pentameric bundle

The results indicate that the helices in the pentameric bundles are strongly tilted having the largest inter-helical distance. A straightening will not allow a water filled column to exist. The lower tilt angles of the tetra and hexameric bundles match NMR spectroscopic data on equivalent single peptides in equivalent lipids [50,51] and consecutive MD simulations [51]. A series of MD simulations on the TMD of Vpu in various lipid bilayer systems have shown that there is no simple correlation between tilt angle and lipid thickness [23]. Often the tilt shows rather large fluctuations and a mismatch is compensated by an alternating kink angle. With Lys-2 and Arg-22 and their flexible and extended side chains [52] at either end of the TMD a large tilt in the pentameric assembly is by all means possible for the 8a peptide

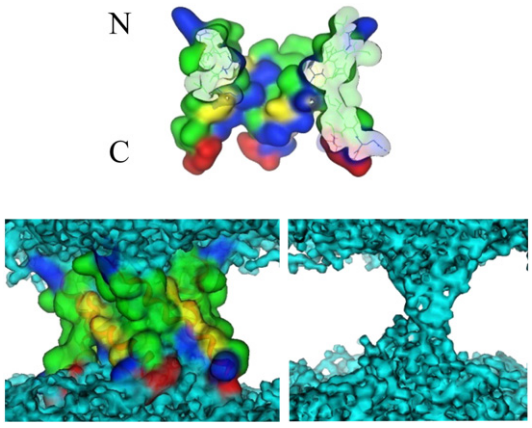

Fig. 5. Cross-section view of PBM2 (see Fig. 4) after 15 ns of MD simulation shown in a 'Gaussian Contact' mode (MOE) (top). Hydrophilic residues (Lys-2, Thr-8, Ser-11, Ser-14 and Thr-18) are highlighted in blue, hydrophobic residues in green, cysteines in yellow and Arg-22 in red. Outside view of the same bundle with lipid molecules omitted for clarity (lower left). The water molecules are shown in blue. Graphical representation of only the water column within the bundle model (lower right).

bundle. Computational studies on a model including the extramembrane parts are necessary to further evaluate the shape of the 'proper' bundle.

4.6. Discrimination between the bundle models

One the bases of the applied assembly protocol a pentameric bundle is harboring a column of water molecules during the extended equilibration of a MD simulation. All other models lose their circular assembly structure by approaching each other as if the pore is 'squeezed'. A similar situation has been reported also for simulations on the TMDs of Vpu from HIV-1 [53]. The size of the pore in the PBMs would allow the physiological relevant ions to pass. The existence of a continuous water column in a particular bundle model may of course not be the exclusive criteria. Functional studies will be the next level of screening.

4.7. Putative transition between PBM2 and PBM3

There is no possibility for the two bundles PBM2 and PBM3 to interchange based on the energy landscape. It only needs minor changes in the tilt and distance towards the central axis, but the rotational change of almost 180° has to cross a larger barrier (Fig. 3A, middle column) in order to transform PBM2 into PBM3. It needs further computational functional analysis to discriminate between the models such as simulating the passage of an ion through each of the pore and evaluating the potential of the mean force [41]. At this stage it is suggested that both models would be present if generated under the present experimental conditions. This may reflect the situation in vivo, assuming that the proteins first diffuse by themselves freely for a short while until they are finally assembled. In case of an instant assembly at the site of in vivo production in the endoplasmic reticulum, the conformational available space would be possibly limited and a single model may emerge.

5. Conclusions

The protein 8a encoded by SARS-CoV has a single TMD being able to form weak cation-selective channels most likely in a pentameric homomeric assembly. Computational models of the assembled TMD reveal that a pentameric bundle is most likely to harbor a continuous water column. In such a bundle model a polarizable cysteine residue and hydrophilic residues such as serines and threonines are facing the pore. The putative water filled pentameric bundle of the TMD of 8a should be made of helices positioned in an approximately 11 Å distance in respect to their helical long axis and with a tilt of about +40°.

Supplementary materials related to this article can be found online at doi:10.1016/j.bbamem.2010.08.004.

Acknowledgements

WBF acknowledges the National Yang-Ming University and the Government of Taiwan for financial support (Aim of Excellence Program), as well as the National Science Council of Taiwan (NSC). JK acknowledges a fellowship granted jointly by the Alexander von Humboldt-Foundation and NSC.

References

[1] K. Stadler, V. Masignani, M. Eickmann, S. Becker, S. Abrignani, H.-D. Klenk, R. Rappuoli, SARS — beginning to understand a new virus, Nat. Rev. Microbiol. 1 (2003) 209–218.
[2] T.G. Ksiazek, D. Erdman, C.S. Goldsmith, S.R. Zaki, T. Peret, S. Emery, S. Tong, C. Urbani, J.A. Corner, W. Lim, P.E. Rollin, S.F. Dowell, A.-E. Ling, C.D. Humphrey, W.-J. Shieh, J. Guarner, C.D. Paddock, P. Rota, B. Fields, J. DeRisi, J.-Y. Yang, N. Cox, J.M. Hughes, J.W. LeDuc, W.J. Bellini, L.J. Anderson, S.W. Group, A novel coronavirus associated with severe acute respiratory syndrome, New Engl. J. Med. 348 (2003) 1953–1966.
[3] M.A. Marra, S.J.M. Jones, C.R. Astell, R.A. Holt, A. Brooks-Wilson, Y.S.N. Butterfield, J. Khattra, J.K. Asano, S.A. Barber, S.Y. Chan, A. Cloutier, S.M. Coughlin, D. Freeman, N. Girn, O.L. Griffith, S.R. Leach, M. Mayo, H. McDonald, S.B. Montgomery, P.K. Pandoh, A.S. Petrescu, A. Gordon Robertson, J.E. Schein, A. Siddiqui, D.E. Smailus, J. M. Stott, G.S. Yang, F. Plummer, A. Andonov, H. Artsob, N. Bastien, K. Bernard, T.F. Booth, D. Bowness, M. Czub, M. Drebot, L. Fernando, R. Flick, M. Garbutt, M. Gray, A. Grolla, S. Jones, H. Feldmann, A. Meyers, A. Kabani, Y. Li, S. Normand, U. Stroher, G.A. Tipples, S. Tyler, R. Vogrig, D. Ward, B. Watson, R.C. Brunham, M. Krajden, M. Petric, D.M. Skowronski, C. Upton, R.L. Roper, The genome sequence of the SARS-associated coronavirus, Science 300 (2003) 1399–1404.
[4] P.A. Rota, M.S. Oberste, S.S. Monroe, W.A. Nix, R. Campagnoli, J.P. Icenogle, S. Peñaranda, B. Bankamp, K. Maher, M.-H. Chen, S. Tong, A. Tamin, L. Lowe, M. Frace, J.L. DeRisi, Q. Chen, D. Wang, D.D. Erdman, T.C.T. Peret, C. Burns, T.G. Ksiazek, P.E. Rollin, A. Sanchez, S. Liffick, B. Holloway, J. Limor, K. McCaustland, M. Olsen-Rasmussen, R. Fouchier, S. Günther, A.D.M.E. Osterhaus, C. Drosten, M.A. Pallansch, L.J. Anderson, W.J. Bellini, Characterization of a novel coronavirus associated with severe acute respiratory syndrome, Science 300 (2003) 1394–1399.
[5] Y. Guan, B.-J. Zheng, Y.Q. He, X.L. Liu, Z.X. Zhuang, C.L. Cheung, S.W. Luo, P.H. Li, L.J. Zhang, Y.J. Huan, K.M. Butt, K.L. Wong, K.W. Chan, W. Lim, K.F. Shortrige, K.Y. Yuen, J.S.M. Peiris, L.L.M. Poon, Isolation and characterization of viruses related to the SARS coronavirus from animals in southern China, Science 302 (2003) 276–278.
[6] W.B. Fischer, M.S.P. Sansom, Viral ion channels: structure and function, Biochim. Biophys. Acta 1561 (2002) 27–45.
[7] M.E. Gonzales, L. Carrasco, Viroporins, FEBS Lett. 552 (2003) 28–34.
[8] M. Montal, Structure–function correlates of Vpu, a membrane protein of HIV-1, FEBS Lett. 552 (2003) 47–53.
[9] W.B. Fischer, J. Krüger, Viral channel forming proteins, Int. Rev. Cell Mol. Biol. 275 (2009) 35–63.
[10] K.J. Hallock, D.-K. Lee, J. Omnaas, H.I. Mosberg, A. Ramamoorthy, Membrane composition determines paradixin's mechanism of bilayer disruption, Biophys. J. 83 (2002) 1004–1013.
[11] F. Porcelli, B. Buck, D.-K. Lee, K.J. Hallock, A. Ramamoorthy, G. Veglia, Structure and orientation of pardaxin determined by NMR experiments in model membranes, J. Biol. Chem. 279 (2004) 45815–45823.
[12] J. Pan, S. Tristram-Nagle, J.F. Nagle, Alamethicin aggregation in lipid membranes, J. Membr. Biol. 231 (2009) 11–27.
[13] A. Bhunia, P.N. Domadia, J. Torres, K.J. Hallock, A. Ramamoorthy, S. Bhattachariya, NMR structure of pardaxin, a pore-forming antimicrobial peptide, in lipopolysaccharide micelles. Mechanism of outer membrane permeabilization, J. Biol. Chem. 285 (2010) 3883–3895.
[14] W. Lu, B.-J. Zheng, K. Xu, W. Schwarz, L. Du, C.K.L. Wong, J. Chen, S. Duan, V. Deubel, B. Sun, Severe acute respiratory syndrome-associated coronavirus 3a protein forms an ion channel and modulates virus release, Proc. Natl Acad. Sci. USA 103 (2006) 12540–12545.
[15] J.-L. Popot, D.M. Engelman, Membrane protein folding and oligomerization: the two-stage model, Biochemistry 29 (1990) 4031–4037.
[16] D.M. Engelman, Y. Chen, C.-N. Chin, A.R. Curran, A.M. Dixon, A.D. Dupuy, A.S. Lee, U. Lehnert, E.E. Matthews, Y.K. Reshetnyak, A. Senes, J.-L. Popot, Membrane protein folding: beyond the two stage model, FEBS Lett. 555 (2003) 122–125.
[17] T. Mehnert, Y.H. Lam, P.J. Judge, A. Routh, D. Fischer, A. Watts, W.B. Fischer, Towards a mechanism of function of the viral ion channel Vpu from HIV-1, J. Biomol. Struct. Dyn. 24 (2007) 589–596.
[18] M. Cserzö, E. Wallin, I. Simon, G. Von Heijne, A. Elofsson, Prediction of transmembrane alpha-helices in procariotic membrane proteins: the Dense Alignment Surface method, Prot. Eng. 10 (1997) 673–676.
[19] E.L. Sonnhammer, G. von Heijne, A. Krogh, A hidden Markov model for predicting transmembrane helices in protein sequences, Proc. Int. Conf. Intell. Syst. Mol. Biol. 6 (1998) 175–182.
[20] K. Hofmann, W. Stoffel, TMbase — a database of membrane spanning protein segments, Biol. Chem. Hoppe Seyler 374 (1993) 166.
[21] D. Juretic, L. Zoranic, D. Zucic, Basic charge clusters and prediction of membrane protein topology, J. Chem. Inf. Comput. Sci. 42 (2002) 620–632.
[22] T. Hirokawa, S. Boon-Chieng, S. Mitaku, SOSUI: classification and secondary structure prediction system for membrane proteins, Bioinformatics 14 (1998) 378–379.
[23] J. Krüger, W.B. Fischer, Exploring the conformational space of Vpu from HIV-1: a versatile and adaptable protein, J. Comp. Chem. 29 (2008) 2416–2424.
[24] J. Krüger, W.B. Fischer, Assembly of viral membrane proteins, J. Chem. Theory Comput. 5 (2009) 2503–2513.
[25] T. Mehnert, A. Routh, P.J. Judge, Y.H. Lam, D. Fischer, A. Watts, W.B. Fischer, Biophysical characterisation of Vpu from HIV-1 suggests a channel-pore dualism, Proteins 70 (2008) 1488–1497.
[26] M. Pawlak, S. Stankowski, G. Schwarz, Melittin induced voltage-dependent conductance in DOPC lipid bilayers, Biochim. Biophys. Acta 1062 (1991) 94–102.
[27] L. Mereuta, T. Luchian, Y. Park, K.-S. Hahm, The role played by lipids unsaturation upon the membrane interaction of the *Heliobacter pylori* HP(2–20) antimicrobial peptide analogue HPA3, J. Bioenerg. Biomembr. 41 (2009) 79–84.
[28] U. Schubert, A.V. Ferrer-Montiel, M. Oblatt-Montal, P. Henklein, K. Strebel, M. Montal, Identification of an ion channel activity of the Vpu transmembrane domain and its involvement in the regulation of virus release from HIV-1-infected cells, FEBS Lett. 398 (1996) 12–18.
[29] G.D. Ewart, T. Sutherland, P.W. Gage, G.B. Cox, The Vpu protein of human immunodeficiency virus type 1 forms cation-selective ion channels, J. Virol. 70 (1996) 7108–7115.

[30] A. Premkumar, L. Wilson, G.D. Ewart, P.W. Gage, Cation-selective ion channels formed by p7 of hepatitis C virus are blocked by hexamethylene amiloride, FEBS Lett. 557 (2004) 99–103.
[31] M.L. Chapman, H.M.A. VanDongen, A.M.J. VanDongen, Activation-dependent subconductance levels in the drk1 K channel suggest a subunit basis for ion permeation and gating, Biophys. J. 72 (1997) 708–719.
[32] R.A. Engh, R. Huber, Accurate bond and angle parameter for X-ray protein–structure refinement, Acta Crystallogr. A 47 (1991).
[33] J.-P. Duneau, S. Crouzy, N. Garnier, Y. Chapron, M. Genest, Molecular dynamics simulations of the ErbB-2 transmembrane domain within an explicite membrane environment: comparison with vacuum simulations, Biophys. Chem. 76 (1999) 35–53.
[34] J. Torres, A. Kukol, I.T. Arkin, Mapping the energy surface of transmembrane helix–helix interactions, Biophys. J. 81 (2001) 2681–2692.
[35] A. Kukol, P.D. Adams, L.M. Rice, A.T. Brunger, I.T. Arkin, Experimentally based orientational refinement of membrane protein models: a structure for the influenza A M2 H^+ channel, J. Mol. Biol. 286 (1999) 951–962.
[36] F. Cordes, A. Kukol, L.R. Forrest, I.T. Arkin, M.S.P. Sansom, W.B. Fischer, The structure of the HIV-1 Vpu ion channel: modelling and simulation studies, Biochim. Biophys. Acta 1512 (2001) 291–298.
[37] L. Bu, W. Im, C.L. Brooks III, Membrane assembly of simple helix homo-oligomers studied *via* molecular dynamics simulations, Biophys. J. 92 (2007) 854–863.
[38] S. Faham, D. Yang, E. Bare, S. Yohannan, J.P. Whitelegge, J.U. Bowie, Side-chain contributions to membrane protein structure and stability, J. Mol. Biol. 335 (2004) 297–305.
[39] J.U. Bowie, Solving the membrane protein folding problem, Nature 438 (2005) 581–589.
[40] F.S. Cordes, A. Tustian, M.S.P. Sansom, A. Watts, W.B. Fischer, Bundles consisting of extended transmembrane segments of Vpu from HIV-1: computer simulations and conductance measurements, Biochemistry 41 (2002) 7359–7365.
[41] G. Patargias, H. Martay, W.B. Fischer, Reconstructing potentials of mean force from short steered molecular dynamics simulations of Vpu from HIV-1, J. Biomol. Struc. Dyn. 26 (2009) 1–12.
[42] R.J.C. Hilf, R. Dutzler, Structure of a potentially open state of a proton-activated pentameric ligand-gated ion channel, Nature 457 (2009) 115–119.
[43] R.J. Leonard, C.G. Labarca, P. Charnet, N. Davidson, H.A. Lester, Evidence that the M2 membrane-spanning region lines the ion channel pore of the nicotinic receptor, Science 242 (1988) 1578–1581.
[44] S. Oiki, V. Madison, M. Montal, Bundles of amphipathic transmembrane a-helices as a structural motif for ion-conducting channel proteins: studies on sodium channels and acetylcholine receptors, Proteins 8 (1990) 226–236.
[45] J.V. Melton, G.D. Ewart, R.C. Weir, P.G. Board, E. Lee, P.W. Gage, Alphavirus 6K proteins form ion channels, J. Biol. Chem. 277 (2002) 46923–46931.
[46] M.D. Slugoski, A.M.L. Ng, S.Y.M. Yao, K.M. Smith, C.C. Lin, J. Zhang, E. Karpinski, C.E. Cass, S.A. Baldwin, J.D. Young, A proton-mediated conformational shift identifies a mobile pore-lining cysteine residue (Cys-561) in human concentrative nucleoside transporter 3, J. Biol. Chem. 283 (2008) 8496–8507.
[47] Z.-Z. Mei, H.-J. Mao, L.-H. Jiang, Conserved cysteine residues in the pore region are obligatory for human TRPM2 channel function, Am. J. Physiol. Cell Physiol. 291 (2006) C1022–C1028.
[48] T. Kuner, C. Beck, B. Sakmann, P.H. Seeburg, Channel-lining residues of the AMPA receptor M2 segment: structural environment of the Q/R site and identification of the selectivity filter, J. Neurosci. 21 (2001) 4162–4172.
[49] S.K. Kandasamy, D.-K. Lee, R.P.R. Nanga, J. Xu, J.S. Santos, R.G. Larson, A. Ramamoorthy, Solid-state NMR and molecular dynamics simulations reveal the oligomeric ion-channels of TM2-$GABA_A$ stabilized by intermolecular hydrogen bonding, Biochim. Biophys. Acta 1788 (2009) 686–695.
[50] S.H. Park, S.J. Opella, Tilt angle of a trans-membrane helix is determined by hydrophobic mismatch, J. Mol. Biol. 350 (2005) 310–318.
[51] A. Ramamoorthy, S.K. Kandasamy, D.-K. Lee, S. Kidambi, R.G. Larson, Structure, topology, and tilt of cell-signaling peptides containing nuclear localization sequences in membrane bilayers determined by solid-state NMR and molecular dynamics simulation studies, Biochemistry 46 (2007) 965–975.
[52] E. Strandberg, J.A. Killian, Snorkeling of lysine side chains in transmembrane helices: how easy can it get? FEBS Lett. 544 (2003).
[53] P.B. Moore, Q. Zhong, T. Husslein, M.L. Klein, Simulation of the HIV-1 Vpu transmembrane domain as a pentameric bundle, FEBS Lett. 431 (1998) 143–148.